Minerals **2014**, *4*, 477-502; doi:10.3390/min4020477

OPEN ACCESS

minerals

ISSN 2075-163X
www.mdpi.com/journal/minerals

Article

Jarosite *versus* Soluble Iron-Sulfate Formation and Their Role in Acid Mine Drainage Formation at the Pan de Azúcar Mine Tailings (Zn-Pb-Ag), NW Argentina

Jesica Murray [1,*], Alicia Kirschbaum [1], Bernhard Dold [2], Edi Mendes Guimaraes [3] and Elisa Pannunzio Miner [4]

[1] Instituto de Bio y Geo Ciencias del Noroeste Argentino-Consejo Nacional de Investigaciones Científicas y Técnicas (IBIGEO-CONICET), Museo de Ciencias Naturales, Universidad Nacional de Salta, Mendoza 2, Salta 4400, Argentina; E-Mail: alikir2003@yahoo.com.ar

[2] SUMIRCO (Sustainable Mining Research & Consult EIRL), Casilla 28, San Pedro de la Paz 4130000, Chile; E-Mail: bernhard.dold@gmail.com

[3] Laboratório de Raios-X, Instituto de Geociencias, Universidade de Brasilia (UnB), Brasilia 70910-900, Brasil; E-Mail: rxedi@unb.br

[4] INFQC-CONICET, Facultad de Ciencias Químicas, Universidad Nacional de Córdoba, Córdoba 5000, Argentina; E-Mail: eminer@fcq.unc.edu.ar or hamsterquatch@gmail.com

* Author to whom correspondence should be addressed; E-Mail: jesimurray@yahoo.com.ar; Tel.: +54-387-590-1429.

Received: 28 February 2014; in revised form: 12 May 2014 / Accepted: 19 May 2014 / Published: 30 May 2014

Abstract: Secondary jarosite and water-soluble iron-sulfate minerals control the composition of acid mine waters formed by the oxidation of sulfide in tailings impoundments at the (Zn-Pb-Ag) Pan de Azúcar mine located in the Pozuelos Lagoon Basin (semi-arid climate) in Northwest (NW) Argentina. In the primary zone of the tailings (9.5 wt % pyrite-marcasite) precipitation of anglesite ($PbSO_4$), wupatkite ($(Co,Mg,Ni)Al_2(SO_4)_4$) and gypsum retain Pb, Co and Ca, while mainly Fe^{2+}, Zn^{2+}, Al^{3+}, Mg^{2+}, $As^{3+/5+}$ and Cd^{2+} migrate downwards, forming a sulfate and metal-rich plume. In the oxidation zone, jarosite ($MFe_3(TO_4)_2(OH)_6$) is the main secondary Fe^{3+} phase; its most suitable composition is M = K^+, Na^+, and $Pb^{2+}$and TO_4 = SO_4^{2-}; AsO_4^{2-}. During the dry season, iron-sulfate salts precipitate by capillary transport on the tailings and at the foot of DC2 (tailings impoundment DC2) tailings dam where an acid, Fe^{2+} rich plume outcrops. The most abundant compounds in the acid mine drainage (AMD) are SO_4^{2-}, Fe^{2+}, Fe^{3+},

Zn^{2+}, Al^{3+}, Mg^{2+}, Cu^{2+}, $As^{3+/5+}$, Cd^{2+}. These show peak concentrations at the beginning of the wet season, when the soluble salts and jarosite dissolve. The formation of soluble sulfate salts during the dry season and dilution during the wet season conform an annual cycle of rapid metals and acidity transference from the tailings to the downstream environment.

Keywords: sulfide oxidation; mine tailings; soluble iron-sulfate salts; jarosite; semi-arid climate; metal release; acid mine drainage; environmental implications

1. Introduction

In sulfidic rocks, coal, metallic ore deposits and mine wastes, sulfide mineral oxidation generates the formation of insoluble and water-soluble metal bearing sulfates [1,2]. The presence of efflorescent salts associated with dry periods or hyper arid climates is common [3,4]. The most distinctive characteristics of iron-sulfate salts in these types of environments are their capacity to store metals and acidity, high solubility, and occurrence affected by seasonal variation of the climate. The formation and dissolution of these metal-sulfates play an important role in the storage and transport of acidity and metals [2,5,6]. The dissolution of efflorescent salts influences the composition of acid mine waters, which affect water quality, and aquatic life and contaminate fluvial sediments downstream and in the surrounding areas [7,8].

The composition of the salts reflects the chemistry of the evaporated waters from which they were formed, including information about the pH conditions during formation. Therefore, identification of efflorescent salts can provide information about water quality and water-rock interaction; they are direct evidence of the pathways of sulfide oxidation and the reactions that occurred in the alteration of the associated assemblages [2].

Many of the soluble minerals (here we refer to minerals that rapidly dissolve in contact with water) have the simplified formula $MSO_4 \cdot nH_2O$, wherein *M* represents divalent Fe, Mn, Co, Ni, Mg, Cu or Zn, and *n* ranges from 1 to 7. The melanterite group is one of the most representative. Sulfates formed by trivalent cations are also common and are characterized by the general formula $A_2(SO_4)_3 \cdot nH_2O$, where $A = Al^{3+}$ or Fe^{3+}, and *n* ranges from 6 to 17; for this group, coquimbite ($Fe_2(SO_4)_3 \cdot 9H_2O$) and alunogen ($Al_2(SO_4)_3 \cdot 17H_2O$) are the most frequent phases [2]. There are also some sulfates with mixed

divalent–trivalent metal ions in their composition, the general formula is $AR_2(SO_4)_2 \cdot nH_2O$, where *A* is Mg^{2+}, Fe^{2+}, Mn^{2+}, Co^{2+}, or Zn^{2+} and *R* is Al^{3+}, Fe^{3+}, or Cr^{3+}; the halotrichite group is the most frequently reported [7,9]. There is also a group of OH-bearing minerals known as the copiapite group with the formula $AR_2(SO_4)_6(OH)_2 \cdot 20H_2O$. Minerals from this group are some of the most common soluble salts derived from the oxidation of sulfides [2,10].

The less soluble sulfate minerals are divided into two groups; the poorly crystalline oxy-hydroxysulfates of Fe and Al, such as schwertmannite, ferrihydrite, gibbsite, alunogen, *etc.* [11,12], and the well-crystalline minerals, represented by the alunite supergroup, in which the jarosite subgroup is included [2]. The jarosite general formula is $MFe_3(TO_4)_2(OH)_6$ where *M* is Na, K, Ag, Tl, NH_4, H_3O and ½Pb and (TO_4) could be (SO_4), (PO_4), (AsO_4) [13,14]. Its formation occurs in a pH range 1–3 [14]. In sulfide deposits

and mine wastes, jarosite plays an important role because of its ability to remove metals from solution during precipitation [9,15].

Pan de Azúcar ceased activity twenty years ago, exposing pyrite-marcasite rich tailings impoundments to weathering. As a result, secondary soluble and insoluble sulfate minerals and acid mine drainage (AMD) have formed. The strongly seasonal climate in the region favors the formation of soluble iron-sulfate salts during the dry season and their dissolution in the wet season. This process is thought to be primarily responsible for generating acidity and metals in the Pozuelos basin. In the region there are other similar inactive sulfide mining sites, such as the La Concordia mine and the La Poma mineral treatment plant. These abandoned sites show evidence of advanced sulfide oxidation, soluble sulfate-salt formation and acid mine drainage generation, causing an increase the metal load of the waters [16]. This paper presents information about sulfide oxidation in tailings from Zn-Pb-Ag mining in a semi-arid climate with a focus on the cycle of secondary Fe water-soluble and insoluble sulfate formation, including their role in metal mobility and environmental implications.

1.1. Site Location and Description

The Pan de Azúcar mine is situated in the Puna plateau region in Northwest (NW) Argentina at 3700 m altitude above sea level. The mine is located at the head of the Pozuelos Lagoon Basin watershed, 25 km upstream from the Pozuelos Lagoon, which has been declared a National Natural Monument (1980), a United Nations Educational, Scientific, and Cultural Organization (UNESCO) Biosphere Reserve (1990) and a Ramsar Site (1992). One of the main lagoon tributaries is the Cincel River, which drains into the south area of the basin and receives acid drainage from the tailings close to Pan de Azúcar mine (Figure 1).

The climate in the region is controlled by the South American Summer Monsoon system, with annual precipitations of 350 mm [17]. Rainfall is strongly seasonal, with about 70% of the yearly total precipitations during summer (December to March), followed by eight months of dry weather. The annual average temperature is 3–13 °C with high daily thermal fluctuation. South-easterly summer winds are generally weak, whereas westerly winter winds are substantially stronger during the dry season, especially from August to November [18–20]). Pan de Azúcar, with a small number of inhabitants, is the most populated village close to the mine, while downstream there is a smaller village, Cienego Grande (Figure 1). Most of the local economy is based on breeding of endemic camelid (*Vicugna vicugna*, *Lama glama*) and sheep.

1.2. Ore Geology, Mining and Tailings Impoundment History

In Pan de Azúcar, the Zn-Pb-Ag mineralization is hosted in hydrothermal veins emplaced in dacitic rocks, dacitic breccias, and Ordovician sedimentary rocks. Pan de Azúcar was an underground mine that had operated from colonial times until 1990, when the operation ceased without the implementation of any closure plan. Sphalerite, galena (with Ag minerals as inclusions), pyrite and marcasite represent 80% of the sulfide mineralogy. The pyrite content in tailings impoundments was around 9.5 wt %. The remaining 10%–15% of the ore mineralogy was arsenopyrite, bournonite ($(PbCuSb)S_3$), chalcopyrite ($(CuFe)S_2$), stannite ($(Cu_2FeSn)S_4$), freibergite ($(Ag,Cu,Fe)_{12}(SbAs)_4S_{13}$), greenockite (CdS), pyrargyrite ($(Ag_3Sb)S_3$), pyrrhotite ($Fe_{x-1}S$), semseyite ($(Pb_9Sb_8)S_{21}$), wurtzite

((ZnFe)S) gold and native silver. Argyrodite ($(Ag_8Ge)S_6$), boulangerite ($(Pb_5Sb_4)S_{11}$), cassiterite (SnO_2), and electrum were accessories. Quartz, sericite-illite, kaolinite, adularia and scarce calcite were the gangue minerals that hosted the ore. Pb, Zn, and Ag were the metals recovered, and the scale of production was approximately 33 t/day with 7.3 wt % Pb; 5.6 wt % Zn; 461 g/t Ag. During the last mining period (1975–1990), the benefaction process included milling and flotation [21–23]. The tailings impoundments cover an area of 700,000 m^2 without any impermeabilization of the basement (Figure 1). In the beginning, the tailings were discharged downwards from the mine in the direction of the Pan de Azúcar stream (as riverine disposal) without any confinement structure. The first tailings deposited were CN (tailings impoundment CN), afterwards three dams were built with the upstream method, forming the tailings impoundments called DC3 (tailings impoundment DC3), DC2 and DC1 (Figure 1).

Figure 1. Location of Pan de Azúcar mine and its tailings impoundments.

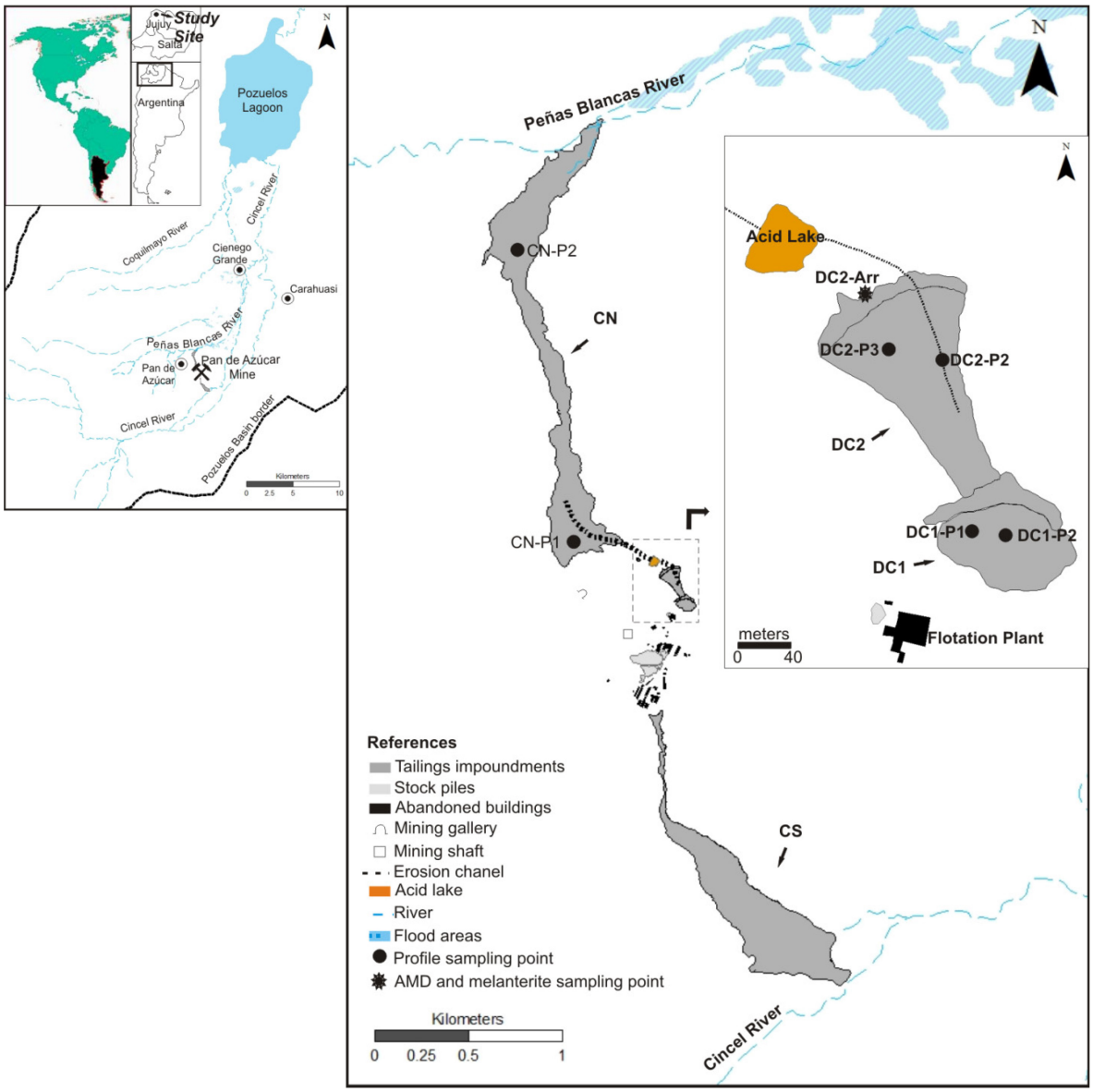

After mine closure, erosion from runoff during wet seasons resulted in a dam failure at the DC3 dam; its tailings flushed downstream, covering the tailings of CN. Then, fluvial erosion produced a channel in the surface of DC2 and its sediments also flowed downstream. A deep erosion channel

(2 m high), which reached the basement of the tailings and crossed its whole surface from south to north was formed in DC2 (Figure 1). After each rainy season, the surface of the erosion channel wall is completely covered by efflorescent salts formed by the evaporation of pore water in contact with air. Moreover, sulfate salts such as melanterite precipitates at the foot of DC2, where rich ferrous iron acid waters outcrop (Figures 2 and 3).

In 2010, the DC3 dam was repaired by the Jujuy provincial Environment Agency by the construction of a dacitic rock wall approximately 2 m in height. Consequently, during the wet season, acid water that drains from DC1 and DC2 now forms an acid pond of approximately 2000 m^2 in DC 3 (Figure 4a). Because of the reconstruction of the DC3 dam, CN does not receive further sediments from the upstream tailings. Nevertheless, there are some filtrations in the newly-constructed DC3 dam and acid waters from the lake that drain into CN. The lake becomes completely dry at the end of the dry season (Figure 4c).

Figure 2. Tailings impoundment DC2. (**a**) Picture of the erosion channel originated by fluvial erosion during the rainy season; (**b**) Wall of the erosion channel where a profile of the tailings covered by efflorescent salts is visible; (**c**) Profile DC2-P2 (1.11 m depth) after cleaning its surface, 1 = DC2-P2-1; 2 = DC2-P2-2; 3 = DC2-P2-3; 4 = DC2-P2-4; 5 = DC2-P2-5; (**d**) Yellow efflorescent salts sampled in the oxidation zone (sample DC2-P2-3-E); and (**e**) Yellow and white efflorescent salts sampled in the primary zone (sample DC2-P2-5-E).

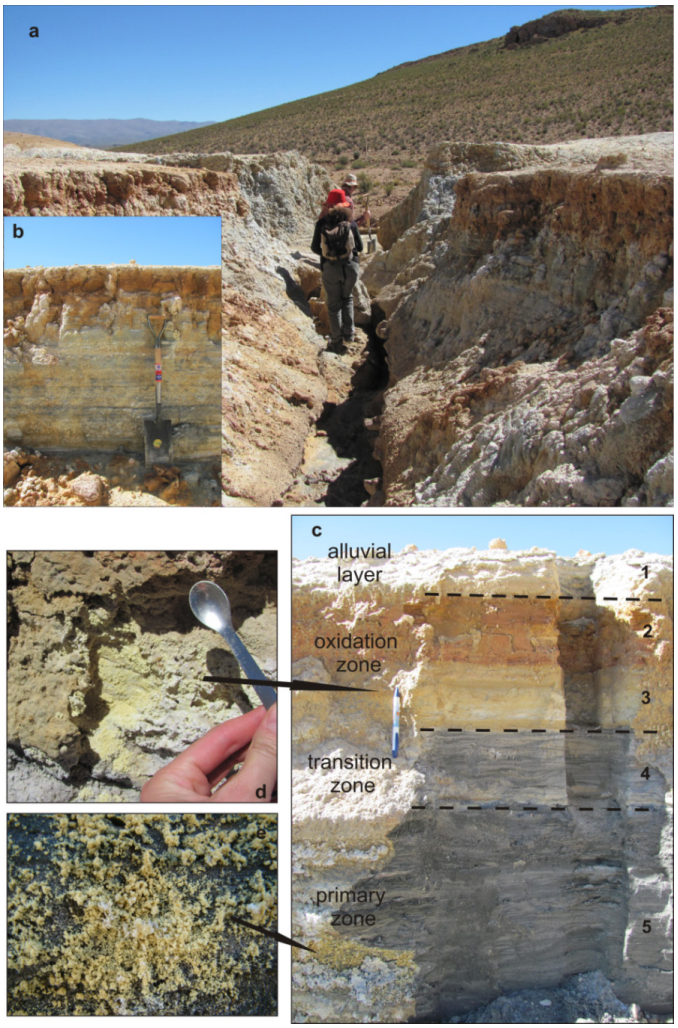

Figure 3. (**a**) Acid waters that seep from the base of the DC2 tailings impoundments. (**b**) Light blue melanterite precipitates. White salts are a product of metalterite dehydration, and correspond to rozenite. And (**c**) Scanning Electron Microscope (SEM) picture for melanterite crystals and alunogen, and Energy Dispersive X-Ray Spectrometer (EDS) lectures for those mineral phases analyzed in Points 1 and 2, respectively.

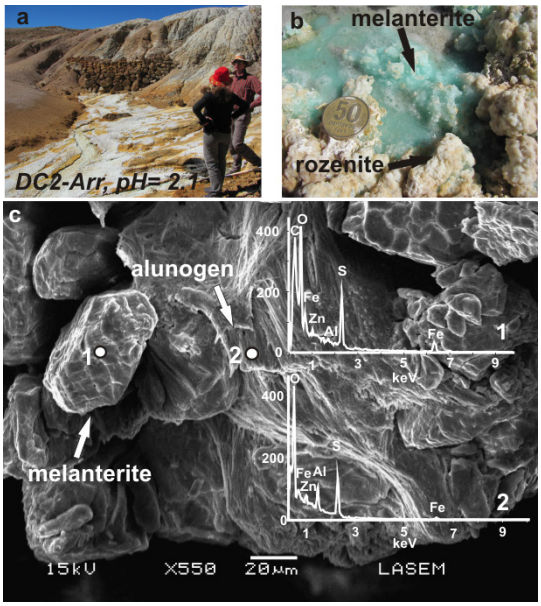

Figure 4. The acid pond on the surface of the tailings impoundments at the Pan de Azúcar mine during the wet and dry seasons. (**a**) T4, end of wet season = sample DC3-L-3 (T4), pH = 3.7; (**b**) T1, during dry season= sample DC3-L-1 (T1), pH = 2.0; (**c**) T2 = lake dried at the end of dry season, pH measurement was not possible; (**d**) T3, beginning of wet season = sample DC3-L-2 (T3), pH = 2.4; and (**e**) Concentration of sulfate and metals (mg/L) for the different periods, scale is logarithmic.

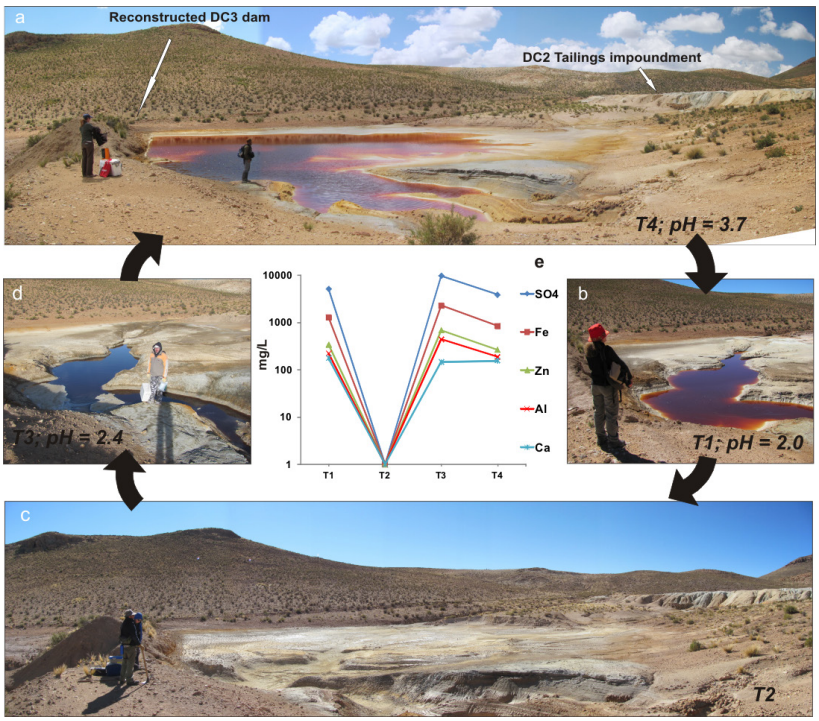

During the wet season, acid waters that drain from CN discharge to the Peñas Blancas River and then into the Cincel River. In the southern area of the mine there is also a surface covered with mine waste (CS; Figure 1), but according to field observations, its sulfide content is lower than in the tailings.

2. Experimental Section

2.1. Sampling and Mineralogical Analysis of Tailings and Efflorescent Salts

The sampling in the tailings was made during the dry seasons of 2011, 2012 and 2013. Pits of approximately 1 m^2 were excavated to the basement (1–1.8 m depth). Six profiles were made in the tailings (DC1-P1; DC1-P2; DC2-P2; DC2-P3; CN-P1 and CN-P2) (Figure 1), a total of 34 tailings samples were taken. The sampling criterion was based on the variation of color, grain size, humidity content, and mineralogy along the oxidation and primary zone. Where necessary, sub-samples were taken. Samples were dried at room temperature and according to the description of mineralogical characteristics, color and grain size estimation was conducted. The dry samples were homogenized and packed into polyethylene bags for storage at room temperature. The pH measurements were obtained in the laboratory by a potentiometric method that is used for soil pH determinations, which consists of a dilution of tailings sediments in deionized water in a solution of 1:2.5 and pH measurement [24].

Sediments from the profile DC2-P2 (DC2-P2-1, 2, 3, 4, 5) were sampled over one of the walls of the erosion channel (Figure 2c).

Efflorescent salts were sampled in three different parts of the mine tailings: (1) From the wall of the erosion channel along the DC2-P2 profile (Figure 2c–e); (2) Salts that precipitate from the acid mine drainage that seep from DC2 (Figure 3a,b); (3) Salts that cover the surface of CN tailings. They were sampled with stainless steel spoons, stored in PVC tubes, rapidly sealed and kept in an ice-packed cooler. Once in the laboratory, they were stored in a refrigerator until analyzed. The sampling of salts along the profile DC2-P2 was made taking the oxidation rate of the tailings along the profile into consideration; each sample corresponded to a different level in the profile (DC2-P2-2-E, 3-E, 4-E, 5a-E and 5b-E).

The mineralogical composition of tailings was determined by polished thin sections from bulk samples and by X-ray diffraction (XRD). Samples from the profiles DC1-P2 and DC2-P2 were analyzed using a PANalytical diffractometer with monochromated CuKα (λ = 1.54056 Å), 4°–70° 2θ, 0.02 step and 10 s per step. These measurements were carried out in X-Ray laboratory at the Institute of Physical-Chemical Investigations of Córdoba (INFIQC, Córdoba, Argentina). Samples from the profile DC2-P3, DC3-P1, CN-P1 and CN-P2 were analyzed by Rigaku-Ultima IX diffractometer (X-Ray laboratory at the Geoscience Institute, Brasilia University, Brasilia, Brazil) with monochromated CuKα (λ = 1.54056 Å); the settings were 4°–70° 2θ, 0.02 step size and 0.6°/min speed. Efflorescent salt determination was also made by the Rigaku-Ultima IX diffractometer with monochromated CuKα (λ = 1.54056 Å); the settings were 2°–70° 2θ, 0.05 step size and 5°/min speed. High speed in the XRD analysis for salts was preferred in order to prevent the mineralogical changes that occur when they are exposed to air.

For tailings mineralogy description, the classification proposed by Jambor (1994) [25] was used, where the term "primary" is used to designate the complete suite of minerals that was initially deposited in the impoundment. The primary suite includes both hypogene and supergene minerals.

"Secondary" minerals are those produced within the tailings after mining and milling as a result of weathering processes. "Tertiary" minerals are those phases formed during sampling, and "quaternary" the ones formed during the storage of samples.

2.2. Scanning Electron Microprobe with EDS Analysis

Investigation of efflorescent salts by Scanning Electron Microprobe (SEM) and Energy Dispersive X-Ray Spectrometer (EDS) analysis were done on the melanterite samples with JOEL (6480LU) equipment at the National University of Salta.

2.3. Sequential Extractions

To study the element speciation in the mine tailings, four samples (DC2-P2-1, 2, 3, 5) from the profile DC2-P2 were subjected to the seven-step sequential extraction procedure described by Dold [26]. Step 1 releases the water-soluble fraction (1.0 g sample into 50 mL deionized H_2O shaken for 1 h at room temperature room temperature (RT)); Step 2 releases the exchangeable fraction (1 M NH_4-acetate, pH 4.5, shaken for 2 h, RT); Step 3 addresses the Fe(III) oxy-hydroxides fraction (0.2 M NH_4-oxalate, pH 3.0, shaken for 1 h in darkness, RT); Step 4 dissolves the Fe(III) oxides fraction (0.2 M NH_4-oxalate, pH 3.0, heat in water bath 80 °C for 2 h); Step 5 consists of a change from a reducing to an oxidizing condition and is performed by an H_2O_2 leach (35% H_2O_2 heat in water bath for 1 h) to oxidize organic matter and dissolve secondary sulfide minerals; Step 6 ($KClO_3$ and HCl, followed by 4 M HNO_3 boiling) dissolves primary sulfides and step 7 (HCl, HF, $HClO_4$, HNO_3) consists of the residual fraction (silicates). The leaches were analyzed by Inductively Coupled Plasma-Optical Emission Spectrometry (ICP-OES) in SGS Laboratory, Ontario, Canada.

2.4. Acid-Base Accounting

The wt % content of marcasite-pyrite, neutral potential, acid potential (NP; AP) and sulfide net neutralization potential (SNNP) were calculated with data from sequential extraction of DC2-P2-1, 2, 3, and 5 samples. The wt % marcasite-pyrite is estimated by the value of wt % $S_{sulfide}$, which is given by the wt % S in Step 6 of the sequential extraction. NP is calculated taking into consideration that the Ca from Step 2 comes from the dissolution of calcite in that step. The sulfide net neutralization potential (SNNP) was calculated with the assumption that at neutral pH, 4 mol of calcite (HCO_3-dominant species at pH 7) is necessary for the neutralization of 4 mol H^+ produced by the oxidation of 1 mol of pyrite.

2.5. Acid Mine Drainage (AMD) and Acid Ponds

Acid water samples were taken from the surface of the acid pond (DC3-L) during the dry and wet seasons and from the acid drainage that seeps from DC2 tailings impoundment during the dry season (DC2-Arr). The samples from the pond correspond to a cycle from dry to wet season for the 2011–2012 period. DC3-L-1-(T1) was taken during the dry season (May 2011), the sample DC3-L-2-(T3) after the first rains at the beginning of the wet season (December 2011), and the sample DC3-L-3-(T4) at the end of the wet season (March 2012).

All the samples were filtered in the field with 0.2 µm Millex HV filtration units using a syringe; the samples were stored at 4 °C in 15 mL polyethylene centrifuge tubes, the samples used for cation analysis were acidified to pH < 2 with suprapure HNO_3 and analyzed by Inductively Coupled Plasma-Mass Spectrometry (ICP-MS) and Inductively Coupled Plasma-Optical Emission Spectrometry (ICP-OES). To determine anions, samples were analyzed by ion chromatography (IC). The pH values were determined in the field with multi-parametric Hanna equipment (Code HI991300N).

3. Results and Discussion

3.1. General Characteristics and Mineralogy of Tailings

3.1.1. Tailings Impoundment DC1

The tailings impoundment DC1 (Figure 1) has a surface of 6800 m^2, and approximately 2 m height. Its surface does not exhibit signs of erosion. Two profiles, DC1-P1 (1.15 m) and DC1-P2, (1.07 m) were measured and sampled in this tailings impoundment (Figure 1). Both profiles have a very similar stratigraphy and features (Figure 5). The upper alluvial layer (DC1-P1 = 5.5; DC1-P2 = 10 cm) is composed of a mixture of primary and secondary mineralogy and alluvial sediments deposited over the tailings due to erosion and remobilization in the tailings surface and the surrounding area. It is underlain by an oxidation zone formed after oxidation of sulfide (Figure 5). It has a low pH (2.5–3.0), is 50–57 cm thick (DC1-P1 = 50.5 cm; DC1-P2 = 57 cm) and has intercalations of orange, pale red, pale brown, and light yellow layers. Directly below is the primary zone, which is dark grey colored with intercalation of some light grey layers. Its pH is also low (2.3).

A detailed mineralogical analysis was made from the DC1-P2 profile. In the oxidation zone, the secondary phases are Fe (III) oxyhydroxydes, most likely schwertmannite (Figure 6), and helmutwinkerite ($Pb(Zn,Cu)_2(AsO_4)_2 \cdot H_2O$), gypsum, jarosite, alunite, and basaluminite, the primary mineralogy is quartz, albite, and illite.

Figure 5. Scheme showing the main features, process, and mineralogy of DC1 tailings impoundment. Abbreviations are gy = gypsum; jt = jarosite; qtz = quartz; ab = albite; ill = illite; kao = kaolinite; py = pyrite; mr = marcasite; sl = sphalerite; gn = galena; asp = arsenopyrite; alu = alunite, basal = basaluminite; helm = helmuntwinkerite; slav = slavikite.

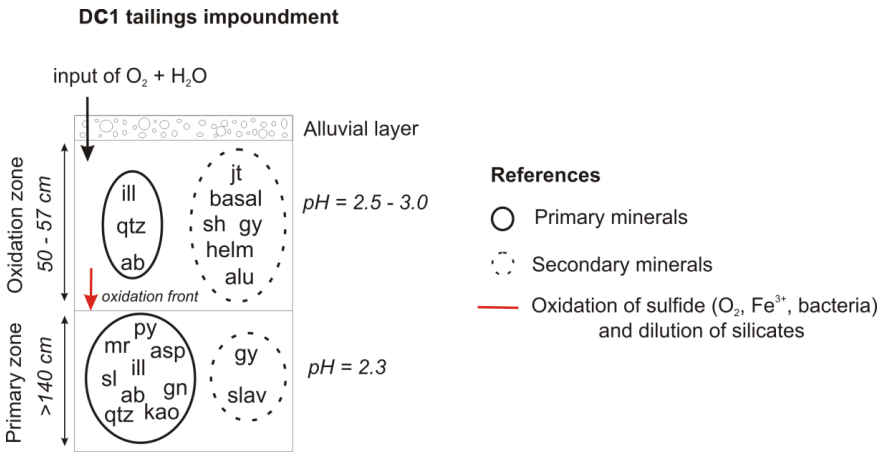

Figure 6. X-ray power diffraction pattern for the bulk sample DC1-P2-3. The arrows indicate the positions (d(Å)) of the main peaks for schwertmannite. The shape and intensities of the two main peaks (2.55 and 1.51 Å) suggest the presence of schwertmannite in this sample.

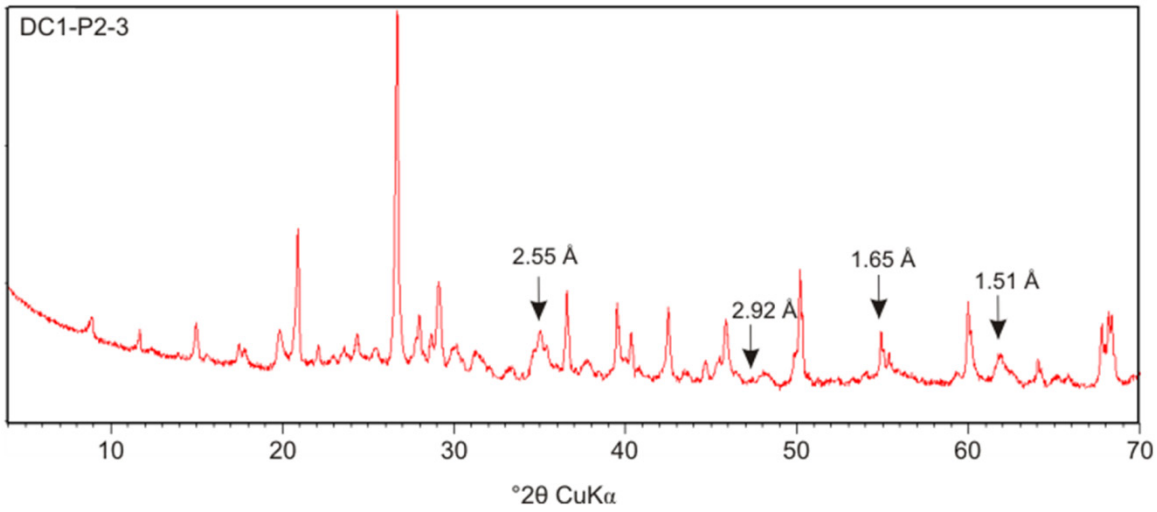

The deepest layer (DC1-P2-4) (54 cm without reaching the basement) corresponds to the primary zone where the primary assemblage is pyrite, marcasite, sphalerite, galene, arsenopyrite, kaolinite, illite, quartz and albite. Gypsum and slavikite ($MgFe_3^{3+}(SO_4)_4(OH)\cdot 18H_2O$) are the secondary phases. No efflorescent salts were identified on the surface of this tailings impoundment due to the presence of the upper alluvial layer, which has coarser grain size and prevents capillary transport (Figure 5). This process is also showed in the Section 3.4, Process 2d and Figure 13a.

3.1.2. Tailings Impoundment DC2

The DC2 tailings impoundment has an area of 11,500 m^2 and a maximum height of 2 m, its surface has been eroded by the runoff during wet seasons. An erosion channel that reaches the basement of the tailings crosses it from south to north, exposing a surface of 336 m^2 of tailings (Figures 1 and 2a). Over that channel surface, evaporation of pore water leads to the formation of iron-sulfate rich efflorescent salts (Figures 2b and 7). Information about its composition and formation process is given in Section 3.2.2. In DC2, two sampling profiles (DC2-P2, DC2-P3) were made (Figure 1). The DC2-P2 profile was made in one of the erosion channel walls (Figure 2c). The main features and mineralogy of DC2 are represented in Figure 7.

The tailings are covered by an upper layer composed of a mixture of primary and secondary minerals and alluvial sediments, it is 11–14 cm thick (DC2-P2 = 14 cm; DC2-P3 = 11 cm). It is underlain by the oxidation zone, which has a low pH (1.9–2.7) and is 35–36 cm thick (DC2-P2= 36 cm; DC2-P3 = 35 cm); two horizons of different colors are present in this zone. The upper layer is orange-brown and pale red while the underlying one is light yellow (Figure 2c). XRD analysis indicates that they are mainly composed of secondary minerals, such as jarosite and gypsum, Fe(III) oxyhydroxides like schwertmannite are probably present in the orange-brown and pale-red layer. Quartz, albite, illite and kaolinite are the primary silicate mineral assemblages in these levels. Underling these is a transition zone with a low pH (1.9–2.2) (DC2-P2 = 16 cm; DC2-P3 = 29 cm thick), which is characterized by a dark grey color with

some white and light grey color horizons; the primary mineralogy is characterized by quartz, sericite, illite and kaolinite accompanied by fractured pyrite, marcasite, galena, and sphalerite. According to the polished sections, these show stronger oxidation than in the primary zone. Gypsum, jarosite, anglesite, and alunogen (DC2-P3) are the secondary minerals present. Coquimbite, which appears in the DC2-P2-4 sample, is probably a quaternary mineral because its origin can be associated with oxidation during the storage of the sample. The primary zone (P2 = 45 cm; P3 = 64 cm thick) is grey to dark-grey up to the base (Figure 2c). The primary mineralogy is dominated by pyrite, marcasite, sphalerite, galena, quartz, illite; and the secondary minerals are anglesite and gypsum. Moreover, wupatkite ($(Co,Mg,Ni)Al_2(SO_4)_4$) and vallerite ($(4(Fe^{2+}Cu^{2+})S\cdot(3(Mg,Al)(OH)_2)$) were found in DC2-P2, indicating that the so-called primary zone is affected by element flow and secondary mineral precipitation from the overlying oxidation and transition zones.

Figure 7. Scheme showing the main features, processes, and mineralogy of DC2 tailings impoundment. Abbreviations are gy = gypsum; jt = jarosite; qtz = quartz; ab = albite; ill = illite; kao = kaolinite; py = pyrite; mr = marcasite; sl = sphalerite; gn = galena; asp = arsenopyrite; wu = wupatkiite; vall = vallerite; al = alunogen, cop = copiapite, coq = coquimbite, rh = rhomboclase, rö = römerite, sz = szomolnokite; mel = melanterite.

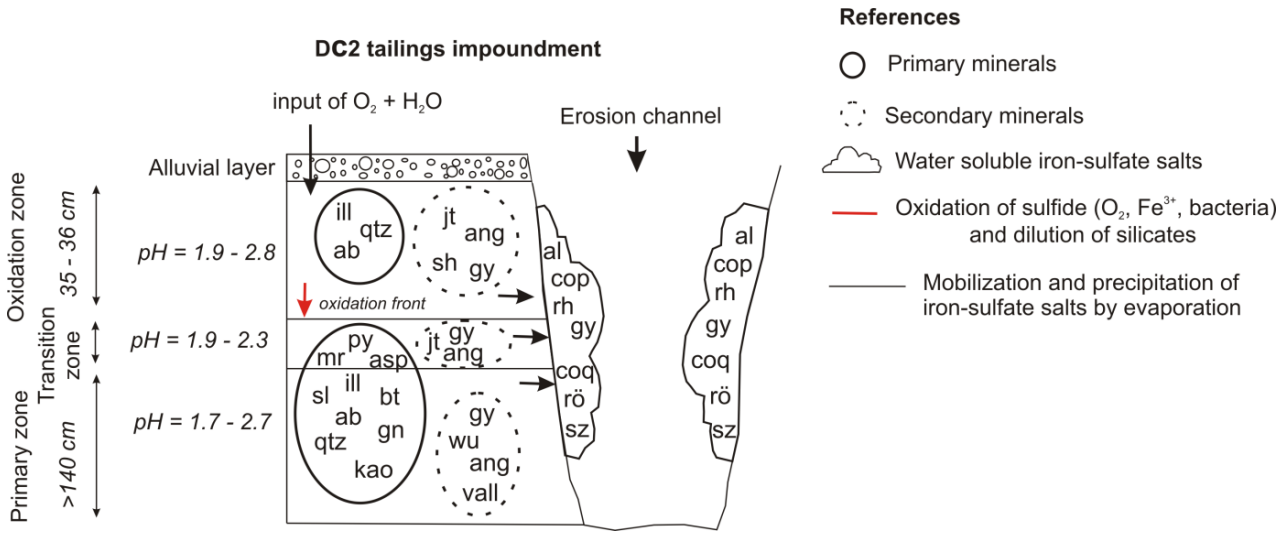

Acid-Base Accounting

The results of the acid-base accounting also confirm the oxidation stratification in the profile DC2-P2 from the tailings impoundment DC2 (Figure 8). The primary zone has a $S_{sulfide}$ content of 5.1 wt % and a calcite equivalent of 0.025 wt %, giving a sulfide net neutralization potential (SNNP) of −319. The tailings, therefore, have a high acid potential (AP). If all $S_{sulfure}$ is assumed to be present as pyrite in the primary zone, the pyrite content is 9.5 wt %.

In the oxidation zone, the SNNP is near zero (DC2-P2-2: −0.31; DC2-P2-3: −1.83) as the AP and neutral potential (NP) have been consumed through oxidation.

Figure 8. Results of sequential extractions from the representative DC2-P2 profile from DC2 tailings impoundment at the Pan de Azúcar mine. For better visibility, the concentration of the residual fraction of K and Al are not shown in this figure. Data including elements that are not shown in this figure are presented in Table S1 (supplementary data).

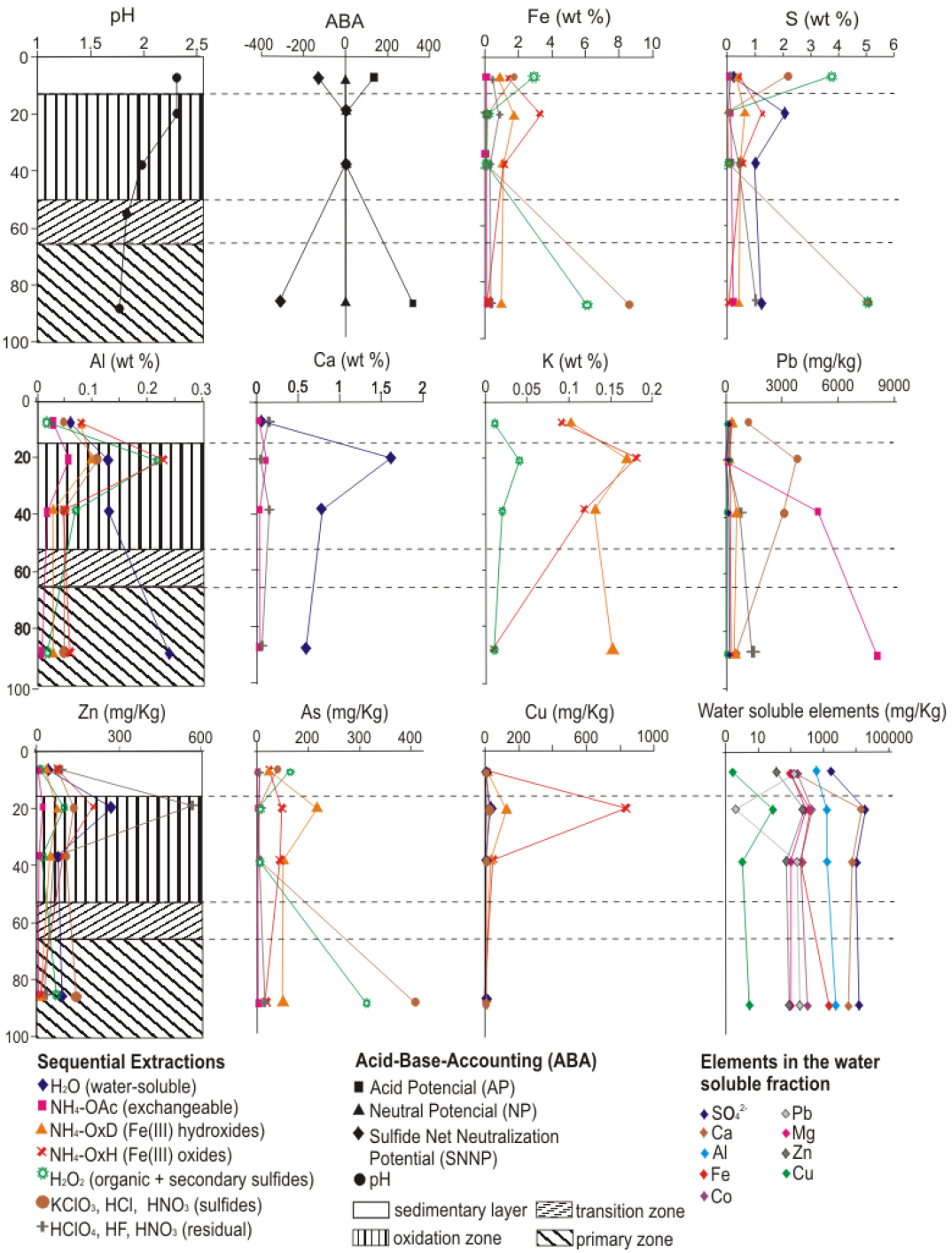

3.1.3. Tailings Impoundment CN

CN covers an area of 393,000 m^2 (Figure 1). It has a maximum thickness of 70 cm in the CN-P1 profile zone and becomes thinner to the north, with a thickness of 30 cm in the CN-P2 profile (Figure 1). These tailings were deposited during the initial operation period of the flotation plant, until the construction of the DC3, DC2, and DC1 dams. At that time, the tailings flow was downstream by

gravity in the direction of the Pan de Azúcar stream. After mine closure, tailings from the erosion of DC3 and DC2 covered the older tailings deposited in CN. Then, the runoff also eroded the surface of CN, remobilizing its sediments and forming an erosion channel that reaches the basement and crosses its surface in the southern area of the tailings (Figure 1).

The stratigraphy of CN is very heterogeneous and varies from south to north, where it is not possible to identify a primary and an oxidation zone, as in the DC1 and DC2 tailings impoundments (Figure 9). In the southern and central area, the sulfide content is higher than in the north, due to gravity deposition closer to the source. The tailings are characterized by an intercalation of layers, composed of medium to coarse grains of quartz, albite, and fragments of rocks with layers of pyrite, marcasite, jarosite and sulfate salts, including copiapite, alunogen, anglesite, and gypsum. As could be observed in the profiles, the presence of efflorescent salts along the whole depth of the tailings is common. In the northern area of CN, the sulfide content is low and the profile is characterized by an intercalation of yellow clay-like layers of jarosite and brownish yellow sandy layers composed of a mixture of silicates, such as quartz, albite and illite, jarosite and sulfate salts like copiapite. The CN surface is partially covered by yellow and white efflorescent salts, which are mainly copiapite, coquimbite, halotrichite, and rhomboclase that were formed by evaporation during the dry season (Figure 9).

Figure 9. Scheme showing the main features, processes, and mineralogy of CN tailings impoundment. These tailings do not present a clear differentiation between an oxidation and a primary zone. Abbreviations are gy = gypsum; jt = jarosite; qtz = quartz; ab = albite; ill = illite; kao = kaolinite; py = pyrite; mr = marcasite; sl = sphalerite; gn = galena; asp = arsenopyrite; al = alunogen, cop = copiapite, coq = coquimbite, gy = gypsum, rh = rhomboclase, hal = halotrichite.

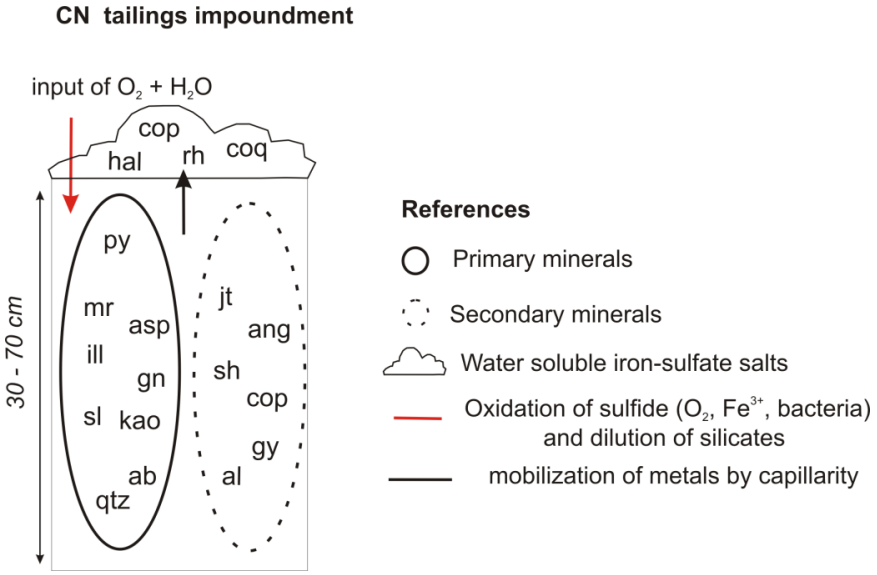

3.2. Secondary Minerals in the Tailings DC1, DC2, CN, and Metals Associations

3.2.1. Insoluble Iron Sulfates

In the oxidation zone of DC1 and DC2, as well as in CN tailings impoundments, jarosite is the main secondary Fe^{3+} phase. The minerals of the jarosite series belong to the jarosite subgroup with the

general formula $MFe_3(TO_4)_2(OH)_6$ [14,15]. According to X-ray diffraction and sequential extraction analysis, the most suitable composition for jarosite at the Pan de Azúcar mine is M = K^+, ½Pb, Na^+, and H_3O^+ and $TO_4 = SO_4^{2-}$; AsO_4^{2-}. Measured pH values in the oxidation and transition zone where its formation took place are 1.9–3, which are in the stability range for jarosite formation [2,9,12,14,27].

The presence of K^+, Pb^{2+} and Na^+, is considered owing to their concentrations in the NH_4-oxalate extractions (Steps 3 and 4) in samples from the oxidation zone. Potassium ranges from 0.12% to 0.18%, lead from 0.058% to 0.015%, and sodium from 0.01% to 0.08% (Figure 8; Table S1). These elements would be provided by illite-sericite, galena and albite, respectively, after oxidation and dilution. For H_3O^+, Dutrizac and Jambor [14] indicate that X-ray diffraction identification patterns of hydronium jarosite are not conclusive because of the similarity of these patterns to those of the alkali jarosites, explaining that these are more stable than the H_3O^+ jarosites. Nevertheless, the presence of H_3O^+ could be associated with the arid climate in the region [14].

X-ray diffraction from samples in the oxidation zone suggests the presence of schwertmannite (Figure 6), a Fe^{3+} oxyhydroxyde sulfate that has also been detected in other tailing impoundments environments [9]. Stoichiometric calculation to approximate the schwertmannite and H_3O^+ jarosites content based on the concentration of K, Pb, Na, and Fe from the steps 3 were made. According to data from Step 3 (Table 1), in the oxidation zone between 32% and 47% of the Fe could be associated to schwertmannite (which dissolves during the Step 3 after the NH_4-oxalate leach in darkness at RT [26]) or to H_3O^+ jarosite.

Therefore, stoichiometric calculations using the value of S to determine the presence of schwertmannite or H_3O^+ jarosite were made (Table 2). The results indicate that S is mainly associated with schwertmannite (Table 2, data in *italics*).

Table 1. Stoichiometric calculations (Calc) of Fe in K, Pb, and Na jarosites (jt) according to the measured (Meas) K, Pb, and Na in Step 3 from sequential extractions from samples DC2-P2-1, DC2-P2-2, DC2-P2-3, DC2-P2-5. The total Fe calculated (Total Calc) for K, Pb, and Na jarosites is compared with the total Fe measured in Step 3; the difference (in bold) represents the Fe from schwertmannite (sh) or H_3O-jt. The percentage of Fe associated with K-jarosite, Na-jarosite and Pb-jarosite, schwertmannite or H_3O-jarosite is also calculated.

Sample	Fe	K-jt	Na-jt	Pb-jt	K-Na-Pb-jt	sh or H_3O-jt
	Step-3	Step-3	Step-3	Step-3	Step-3	Step-3
	Meas (wt %)	Calc (wt %)	Calc (wt %)	Calc (wt %)	Total Calc (wt %)	Cal (wt %)
DC2-P2-1	0.79	0.43	0.04	0.06	0.52	**0.27**
DC2-P2-2	1.70	0.73	0.15	0.02	0.90	**0.80**
DC2-P2-3	1.08	0.56	0.07	0.09	0.73	**0.35**
DC2-P2-5	0.96	0.64	0.04	0.07	0.75	**0.21**

Sample	K-jt	Na-jt	Pb-jt	Total K-Na- Pb-jt	sh or H_3O-jt
	Step-3	Step-3	Step-3	Step-3	Step-3
	Calc (%)	Calc (%)	Calc (%)	Calc (%)	Calc (%)
DC2-P2-1	54.23	4.61	7.53	66.38	**33.61**
DC2-P2-2	42.84	8.57	1.49	52.91	**47.08**
DC2-P2-3	51.57	6.74	8.82	67.14	**32.85**
DC2-P2-5	66.94	3.79	7.71	78.46	**21.54**

Table 2. Stoichiometric calculations (Calc) of S in K, Pb, and Na jarosites (jt) according to the measured (Meas) K, Pb, and Na in Step 3 of the sequential extractions from samples DC2-P2-1, DC2-P2-2, DC2-P2-3, DC2-P2-5. The total S calculated (Total calc) for K, Pb, and Na jarosites is compared with the total S measured in Step 3; the difference (in bold) represents the S from schwertmannite or H3O-jt in Step 3. Results in italic represent the S content measured derived from the schwertmannite dissolution.

Sample	S	K-jt	Na-jt	Pb-jt	K-Na-Pb-jt	sh H_3O-jt	Fe*/S# in sh	S in sh (Fe*/(Fe*/S#))
	Step-3 Meas (wt %)	Step-3 Calc (wt %)	Step-3 Calc (wt %)	Step-3 Calc (wt %)	Step-3 Total Calc (wt %)	Step-3 Cal (wt %)	Meas	Calc (wt %)
DC2-P2-1	0.32	0.16	0.01	0.02	0.20	***0.12***	2.25	***0.12***
DC2-P2-2	0.61	0.28	0.06	0.01	0.34	***0.27***	2.96	***0.27***
DC2-P2-3	0.46	0.21	0.03	0.04	0.28	***0.18***	1.94	***0.18***
DC2-P2-5	0.41	0.25	0.01	0.03	0.29	***0.12***	1.75	***0.12***

Notes: * Fe in schwertmannite or H_3O-jt (Table 1); # S in schwertmannite or H_3O-jt.

The presence of schwertmannite in the oxidation zone of the tailings has implicances in the concentration of arsenic. In the Step 3 of sequential extraction arsenic concentration ranges from 103 to 236 mg/kg and from 92 to 97 mg/kg in the Step 4 (Table S1; Figure 8). Besides arsenic is probably present in the (TO_4) compositional compartments of jarosite, the higher values in the Step 3 denotes the presence of schwertmannite, that can adsorb arsenic due to its high reaction surface [9,28].

In the Section 3.4, the process 2b and the Figure 13a, illustrate that together with arsenic, potassium, sodium and lead are sequestered in the oxidation zone of the tailings because of the formation of jarosite and schwertmannite.

3.2.2. Soluble Sulfates

There is a consistent relationship between the mineralogy of the water-soluble phases in the tailings of the profile DC2-P2 and the composition of the water soluble fraction obtained by sequential extractions for samples DC2-P2-1, 2, 3, 5 (Figure 8). According to the sequential extraction data, S, Ca, Al, Fe, Co, Mg, Zn, and Cu are the most abundant elements in the water soluble fraction (S = 9900–20,900 mg/kg; Ca = 100–15,900 mg/kg; Al = 600–2400 mg/kg; Fe = 90–1500 mg/kg; Co = 157–473 mg/kg; Mg ≤ 100–300 mg/kg); Zn = 37.2–269 mg/kg; Cu = 1.7–29.2 mg/kg) (Figure 4). S is present in the form of SO_4^{2-}; it is the most abundant anion and is present in the composition of all soluble phases. Calcium is mainly concentrated in gypsum ($CaSO_4 \cdot 4H_2O$), and Al, Mg, and Co in wupatkite ($(Co,Mg,Ni)Al_2(SO_4)_4 \cdot 22H_2O$) and alunogen ($Al_2(SO_4)_3 \cdot 17H_2O$).

The high concentrations of Pb in the NH_4-acetate leach (3–8008 mg/kg) in comparison to values in the water soluble fraction (2–199 mg/kg) and the NH_4-oxalate leach (157–589 mg/kg) indicates anglesite dissolution in the NH_4-acetate leach, as proposed by Dold *et al.* [29]. Lead is provided by the oxidation of galena and is associated with anglesite, especially in the primary zone, where this mineral is the main lead sequester (Section 3.4, Process 2a and Figure 13a).

In Step 1 of the sequential extractions, iron is the fourth most abundant metal (Figure 8). However, no water-soluble iron salt was detected by XRD in the bulk tailings samples (Table 2). This can be related to the detection limit of the XRD methodology; phases in low concentration (*i.e.*, <2%–5%) cannot always be identified in bulk sample analysis [30]. Nevertheless, in the erosion channel walls in DC2, the formation of sulfate and Fe-rich efflorescent salts is favored by the exposure of the tailings to air (Section 3.4, Process 2c and Figure 13a). Those salts precipitate directly from the pore water in contact with air, indicating the availability of iron in the tailings pore water.

In the walls of the erosion channel, the color, amount and composition of the salts varies with respect to depth (Figures 2 and 10, and Table 3). Most of these are rich in Fe^{3+}, especially in the oxidation and transition zones, where rhomboclase ($(H_3O)Fe^{3+}(SO_4)_2 \cdot H_2O$) and coquimbite ($Fe^{3+}(SO_4)_3 \cdot 9H_2O$) are the most abundant phases. Copiapite ($Fe^{2+}Fe_4^{3+}(SO_4)_6(OH)_2 \cdot 20H_2O$), which is a mixture of divalent-trivalent Fe salt, is also common. In the primary level (DC2-P2-5), rhomboclase, coquimbite, and copiapite are present; however, there another divalent-trivalent iron salt is detected, römerite ($Fe^{2+}Fe_2^{+3}(SO_4)_4 \cdot 14H_2O$), and an exclusive divalent ferrous phase, which is szomolnokite ($Fe^{2+}SO_4 \cdot H_2O$).

According to Nordstrom and Alpers [1], as long as acid mine water is in contact with pyrite, the dissolved iron will remain in a ferrous state because of the strong reduction capacity of pyrite. Because the oxidation rate is often slow, rapidly flowing mine water will still maintain a high proportion of ferrous iron. The only iron sulfate salts that contain exclusively ferrous iron such as melanterite, rozenite, and szomolnokite are found close to the pyrite sources and associated with more rapidly flowing waters. Ferric-bearing minerals form in more stagnant conditions and are considered hydrologic "dead-ends", where much of the Fe^{2+} has had time to oxidize to Fe^{3+}. This has been confirmed by data from Dold *et al.* [31], which shows that in the oxidation zone, Fe^{3+} is the primarily dominant species. Below the oxidation front, due to microbiological reduction, a plume of ferrous iron enables the iron to mobilize through the tailings stratigraphy. In that process, the reducing bacteria use products of microbial respiration (*i.e.*, low molecular weight carboxylic acids such as acetate and formate) as electron donors and ferric iron as electron sinks [31]. This phenomenon can also be observed in the Acid Rock Drainage (ARD) formation in the Antarctic [32].

The presence of dissolved ferrous iron in the primary zone of the tailings in Pan de Azúcar is confirmed by the presence of soluble Fe^{2+} efflorescent salts in the erosion channel of DC2. Moreover, acidic (pH = 2.1) and colorless water seeps from the base of DC2 (sample DC2-Arr-DS, Table 4) where sulfate, iron, zinc and aluminum are the main compounds (139 g/L SO_4^{2-}; 47.9 g/L Fe (total); 8.96 g/L Zn; 7.12 g/L Al). During the dry season, evaporation leads to the formation of light blue precipitates, which are identified as an assemblage of melanterite-alunogen ($(Fe^{2+},Zn^{2+})SO_4 \cdot 7H_2O$)–($Al_2(SO_4)_3 \cdot 17H_2O$) (Figures 3b,c). This is also showed in the Section 3.4, Processes 3 and 4 presented Figure 13a.

After melanterite precipitates, it dehydrates and turns into white phases, which are identified as rozenite ($(Fe^{2+},Zn^{2+})SO_4 \cdot 4H_2O$) (Figure 3a,b).

A comparison of the composition of the acid water that outcrops at the base of DC2 (sample DC2-Arr) with the composition of the metal concentration in the water-soluble phases in the primary zone (sample DC2-P2-5) (Table 4) indicates that the concentrations of Ca, Co, and Pb decrease considerably in the acid water that discharges from the base of DC2 (Figure 11). As the acid plume

flows downwards in the tailings and gypsum, wupatkite and anglesite precipitates, Ca, Co, and Pb are sequestered by those mineral phases in the flow path (Section 3.4, Process 2a and Figure 13a).

Figure 10. X-ray diffraction (XRD) difractograms for the efflorescent salts in the erosion channel of DC2. al = alunogen, cop = copiapite, coq = coquimbite, gy = gypsum, rh = rhomboclase, rö = römerite, sz = szomolnokite gy = gypsum; jt = jarosite; qtz = quartz.

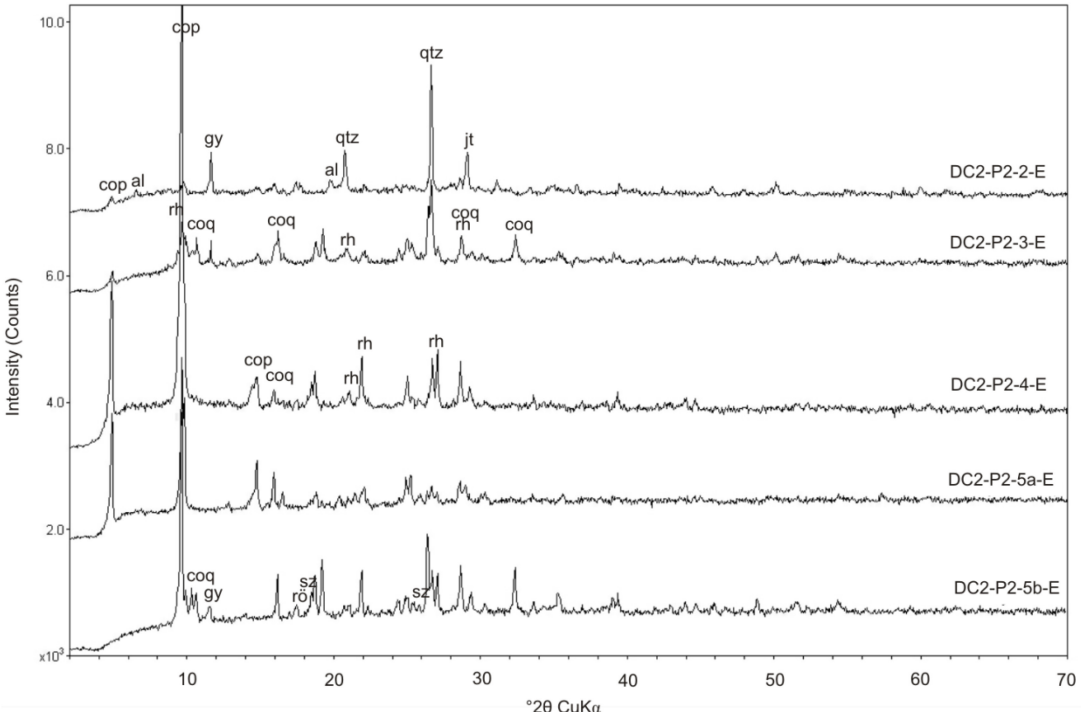

Table 3. Efflorescent salts that cover the tailings in DC2-P2 profile.

Sample	Features	Efflorescent salts and ideal formula
DC2-P2-1-E		No salt formation observed
DC2-P2-2-E	Red-brownish crust with scarce yellow salts	alunogen ($Al_2(SO_4)_3 \cdot 17H_2O$) copiapite ($Fe^{2+}Fe_4^{3+}(SO_4)_6(OH)_2 \cdot 20H_2O$)
DC2-P2-3-E	Predominance of yellow salts, less white	rhomboclase ($(H_3O)Fe^{3+}(SO_4)_2 \cdot H_2O$) coquimbite ($Fe^{3+}(SO_4)_3 \cdot 9H_2O$) copiapite ($Fe^{2+}Fe_4^{3+}(SO_4)_6(OH)_2 \cdot 20H_2O$) gypsum ($CaSO_4) \cdot 4H_2O$
DC2-P2-4-E	Mixture of yellow and white salts	rhomboclase ($(H_3O)Fe^{3+}(SO_4)_2 \cdot H_2O$) copiapite ($Fe^{2+}Fe_4^{3+}(SO_4)_6(OH)_2 \cdot 20H_2O$) coquimbite ($Fe^{3+}(SO_4)_3 \cdot 9H_2O$)
DC2-P2-5a-E	Predominance of yellow salts, less white	copiapite ($Fe^{2+}Fe_4^{3+}(SO_4)_6(OH)_2 \cdot 20H_2O$) rhomboclase ($(H_3O)Fe^{3+}(SO_4)_2 \cdot H_2O$) coquimbite ($Fe^{3+}(SO_4)_3 \cdot 9H_2O$)
DC2-P2-5b-E	Predominance of white salts, less yellow	rhomboclase ($(H_3O)Fe^{3+}(SO_4)_2 \cdot H_2O$) coquimbite ($Fe^{3+}(SO_4)_3 \cdot 9H_2O$) römerite ($Fe^{2+}Fe_2^{+3}(SO_4)_4 \cdot 14H_2O$) szomolnokite ($Fe^{2+}SO_4 \cdot H_2O$) gypsum ($CaSO_4) \cdot 4H_2O$

Table 4. The pH, conductivity, and concentration of sulfate and metals of acid mine drainage (AMD) in mg/L. Conductivity values are given in μS/cm. Data for sample DC2-P2-5, in mg/kg, correspond to the concentration of sulfate and metals in the water-soluble fraction obtained by sequential extractions (see also Table S1).

Parameter	DC2-Arr	DC2-P2-5	DC3-L-1(T1)	DC3-L-2 (T3)	DC3-L-3 (T4)
pH	2.1		2.08	2.42	3.75
Conductivity	>4,000		>4,000	18,470	5,900
	mg/L	mg/kg	mg/L	mg/L	mg/L
SO_4	139,000	122,000	5,130	9,690	3,870
Fe_T	47,900	1,500	1,280	2,270	843
Zn	8,960	88.5	338	686	264
Al	7,120	2,400	222	440	185
Ca	524	5,900	176	146	156
Mg	1,110	100	29	74.5	25.6
Cu	10.1	5.2	17.3	38.8	15.2
As	44.6	<3	4.5	12.2	3.8
Cd	99.7	<1	2.1	5.0	2.4
Pb	1.4	199	1.1	1.8	0.5
Co	9.5	320	0.3	0.8	0.3
Ni	15.2	2.0	0.3	0.7	0.4
Sb	4.7	<5	0.1	0.4	0.1
Cr	1.7	<1	0.2	0.4	0.2
Sn	0.1	0.0	0.0	0.1	0.1

Figure 11. Comparison between the concentration of elements in the water that discharge from the base of DC2 (sample DC2-Arr) and the water-soluble phases in the primary zone from DC2 (sample DC2-P2-5). Concentrations below one for Ca, Co and Pb indicate that they are sequestered in the solid phase.

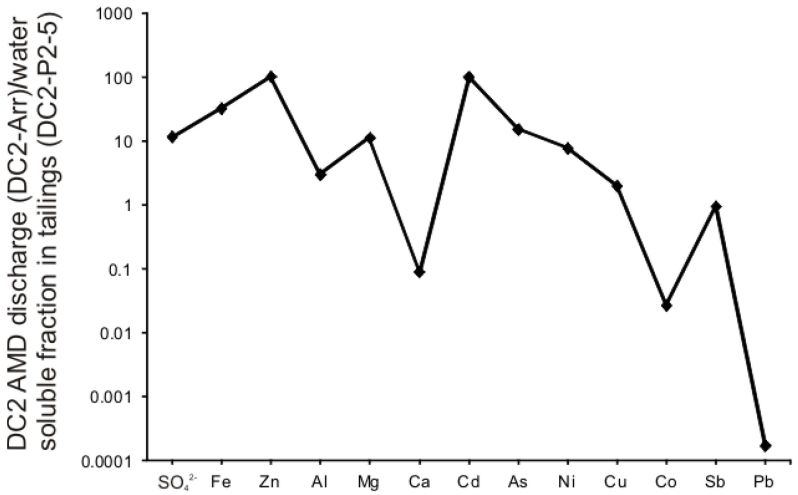

3.2.3. Jarosite and Soluble Fe^{3+} Salt Formation in the Erosion Channel at DC2 Tailings Impoundment

Merwin and Posnjak [33] studied the solubility relationships of minerals in the Fe_2O_3-SO_3-H_2O system at 30–40 °C. This work is still considered to be one of the most extensive works on the ferric

sulfate solubilities [2]. They described a sequence of mineral formation: hydronium-jarosite–butlerite–ferricopiapite–coquimbite–kornelite–rhomboclase in solution conditions at which the pH continually decreases and the solution SO_4/Fe ratio increases (Figure 12).

This phase diagram was used by Jamieson *et al.* [10] to understand jarosite and soluble iron-sulfate formation under different pH, Fe, SO_4 concentrations and evaporation rates at the Richmond mine [1,27]. The authors indicate that throughout the mine, where the formation of iron-sulfate salts prevailed, pH values were low in co-existing water (*i.e.*, pH = −0.9 ± 0.2 (magnesiocopiapite); pH = −2.5 (rhomboclase–römerite); pH = −3.6 (rhomboclase)). Magnesiocopiapite precipitated in a drift a few meters away from K-H_3O jarosites, where there was less evaporation; there the water pH values were ~2 (because of the addition of cool, dilute groundwater from the adjacent host felsic metavolcanic rocks), and had lower Fe and SO_4 concentrations. In this case, jarosite and iron sulfate salt precipitation followed a sequence similar to the one proposed by Merwin and Posnjak [10,27,33].

Figure 12. Solubility relationships of minerals in the Fe_2O_3-SO_3-H_2O system at 30–40 °C. The figure shows the sequence of minerals formation of hydronium-jarosite–butlerite–ferricopiapite–coquimbite–kornelite–rhomboclase in a solution condition in which the pH continually decreases while the solution SO_4/Fe ratio increases. Modified from Merwin and Posnjak [33] in Jambor *et al.* [2]. Reprinted with permission from [2]. Copyright 2000 Mineralogical Society of America.

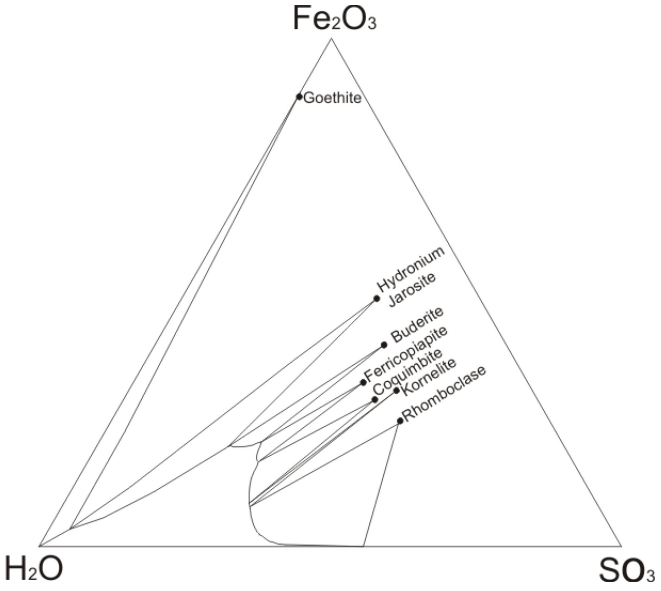

In the case of the Pan de Azúcar tailings impoundments, jarosite is the most abundant secondary phase in the oxidation and transition zone of the tailings, where the evaporation rate is low. The iron-sulfates salts are more abundant in the eroded surface of DC2 tailings, where the pore water rapidly evaporates. The formation conditions for jarosite and iron-sulfates salts could also be explained by the sequence proposed by Merwin and Posnjak [33]. After pyrite and marcasite oxidize and illite and albite dissolve in the tailings stratigraphy, they liberate SO_4^{2-}, Fe^{3+}, K^+, and H^+ into the system; the pH decreases, and jarosite is formed. During this process, more H^+ are liberated, and consequently the pH decreases and the SO_4/Fe ratio increases as an effect of the removal of Fe^{3+} by jarosite precipitation. Then, when pore water comes into direct contact with air, as occurs in the erosion

channel wall of the DC2 tailings impoundment, Fe-sulfate soluble salts will rapidly precipitate in the form of efflorescent salts.

3.2.4. Jarosite and Soluble Fe^{3+} Salts Formation in the CN Tailings

The heterogeneous composition of the tailings in CN along with the absence of a defined primary and oxidation zone, as is found in the DC1 and DC2 tailings impoundments, is related to the deposition history of these areas. In the north area of CN, the sulfide content is low and the tailings are mainly formed by jarosite, intercalated by sand layers of silicates with iron-sulfates salts, such as copiapite. These are the oldest tailings deposited in CN, which originate directly from the flotation plant and are now completely oxidized. The southern area of CN, composed of jarosite and iron-sulfate salts like copiapite, are interlayered with sulfides along the whole depth of tailings. It is covered by secondary and primary minerals from the DC3 and DC2 eroded upstream tailings.

The precipitation of iron-sulfate soluble salts inside the tailings is probably associated with the presence of coarse grain sand layers along the entire CN. These most likely allow a better oxygen supply of the tailings. The formation of yellow and white efflorescent salts such as copiapite, coquimbite, halotrichite, and rhomboclase, which partially cover the surface of CN during the dry season, is possibly favored by evaporation and upwards migration by capillarity of acid sulfate Fe^{3+} rich water pore, as it can be seen in other arid regions [3,9,34].

3.3. Acid Pond Features and Variation in the Water Composition

The acid pond has a maximum depth of approximately 2 m and a maximum surface area of 2000 m^2 at the end of the wet season. Then, water filtration through the DC3 dam and evaporation makes the water level decrease, reaching its lowest level at the end of the dry season, when it becomes completely dry (Figure 4).

The acid pond shows a variation in pH and concentration of sulfate and metals during the course of the year (Table 4, Figure 4). The most abundant compounds in the pond water are SO_4^{2-}, Fe, Zn, and Al, followed by Ca, Mg, Cu, and As (Table 4). The concentration of these elements increases at the beginning of the wet season (T3) by the dissolution of the efflorescent salts rich in SO_4, Fe, Zn, Al, and Ca (copiapite, coquimbite, rhomboclase, alunogen, szomolnokite, gypsum, and Zn-rich melanterite) formed in DC2 during the dry season (Figures 4e and 13a, Process 5). Arsenic content could be provided from the dissolution of jarosite exposed to AMD runoff [35,36] (Figure 13a, Process 6). At the end of the wet season (T4), the pond shows the lowest concentration of sulfate and metals and an increase in its pH value by dilution from rain water. Jarosite precipitates are found at the bottom of the pond as the main secondary mineral that precipitates directly from AMD.

3.4. Conceptual Model for the Cycle of Sulfide Oxidation, Sulfate Formation and Metal Mobility at the Pan de Azúcar Mine; and Possible Pathway of Metals from the Tailings to the Fluvial and Groundwater Systems and on to Pozuelos Lagoon

Figure 13 shows a scheme of the conceptual model proposed for sulfide oxidation, sulfate formation, and metal mobility at the Pan de Azúcar tailings impoundments (a), and the possible

pathway of metals from the tailings to the fluvial and groundwater systems and on to Pozuelos Lagoon (b). The involved processes are described below:

Figure 13. (**a**) Cycle of sulfide oxidation, sulfate formation, and metal mobility at the Pan de Azúcar mine tailings impoundments; and (**b**) Possible pathway of metals from the tailings to the fluvial and ground water systems and then on to Pozuelos Lagoon.

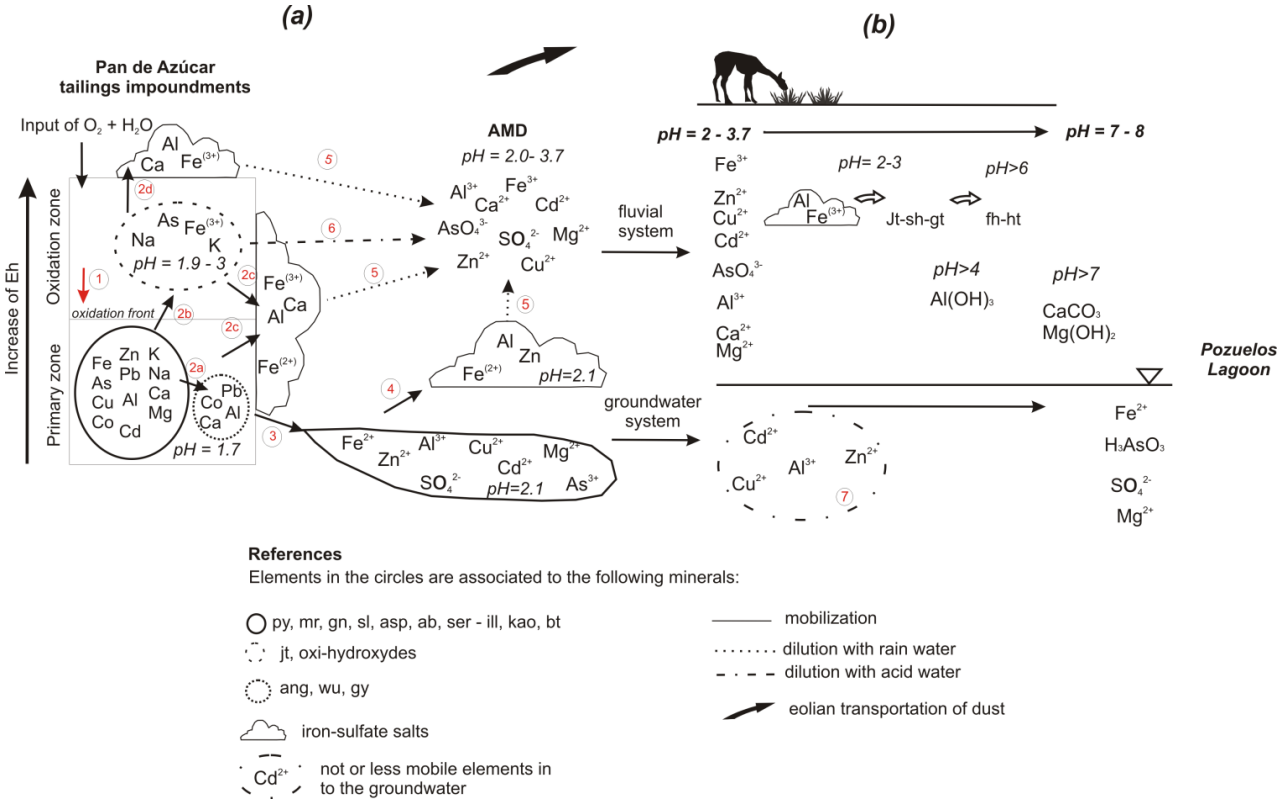

(a) Cycle of sulfide oxidation, sulfate formation, and metal mobility at the Pan de Azúcar mine tailings impoundments.

(1) Oxidation of sulfides (by oxygen, ferric iron, and microbial activity) and dilution of silicates in the oxidation front. Release of sulfate, acidity, iron, metals and alkalis precipitate as secondary minerals or mobilization through the tailings stratigraphy. Below the oxidation front, ferric iron could be reduced again by microbial reducing activity.

(2) Precipitation of sulfates in the tailings:

(2a) In the primary zone of tailings anglesite, wupatkite and gypsum precipitates retain Pb, Co, Ca, and Al. Section 3.2.2.

(2b) Formation of insoluble sulfates in the oxidation zone (jarosite, Fe^{3+} oxy-hydroxyde sulfates like schwertmannite) sequestering mainly As, K and Na. Section 3.2.1.

(2c) After oxidation of sulfide and dilution of silicates in the tailings, sulfate-rich pore water evaporates, allowing the formation of soluble iron sulfates in the wall of the erosion channel in DC2. Alunogen, copiapite, coquimbite, rhomboclase, römerite, gypsum and szomolokite retain mainly Fe^{3+}, Fe^{2+}, Ca, and Al, are the most common phases. Sections 3.2.2 and 3.2.3.

(2d) Precipitation of soluble iron sulfates in the surface of the tailings is produced by the capillarity ascent of metals (copiapite, coquimbite, halotrichite, rhomboclase), which retain mainly Fe^{3+} and Al. Section 3.2.4.

(3) Ferrous iron, sulfate and metals rich AMD plume mobilizes downwards through the primary tailings zone. Section 3.2.2.

(4) AMD plume seeps into the base of the tailings during the dry season, enabling the precipitation of soluble sulfate salts (melanterite, alunogen) and sequestering Fe^{2+}, Zn, and Al. Section 3.2.2.

(5) Dilution of soluble sulfate salts during the wet season, especially during the first rain events. AMD formation and release of SO_4^{2-}, Fe^{2+}, Zn^{2+}, Al^{3+}, Ca^{2+}, Mg^{2+}, Cu^{2+}, Cd^{2+}. Section 3.3.

(6) Dilution of jarosite at pH = 2 by AMD, release of SO_4^{2-}, AsO_4. Section 3.3.

(b) Possible pathway of metals from the tailings to the fluvial and ground water systems and then on to Pozuelos Lagoon.

The main species and metals released into the environment are SO_4^{2-}, Fe^{2+}, Zn^{2+}, Al^{3+}, Mg^{2+}, Cu^{2+}, $As^{3+/5+}$, and Cd^{2+}. In superficial fluvial systems, these elements will precipitate and form a series of oxide-oxyhydroxide sulfate and metal bearing phases. Preliminary field observations indicate that the Peñas Blancas River contains iron-oxides in the fluvial sediments up to at least 5 km downstream from the tailings. Those are probably metal bearing iron-oxides which precipitated directly from AMD, as occurs in other fluvial systems that receive AMD discharge [37–39]. Similarly, the groundwater system also receives an input of metals from the acid plume. In aquifer samples downstream from the mine, the concentration of Cu, Al, Cd, and Zn are below the World Health Organization (WHO) guide levels for drinking water, while arsenic concentrations are above (21–113 μg/L) [40]. Thus, this indicates that metals become immobile when the acid plume reaches the ground water system (7) but arsenic can still migrate because of its speciation as H_3AsO_3. The origin of arsenic could also be related to the natural arsenic background in the region [40,41].

Lead and zinc analysis of soils and plants in the area near the tailings indicate the presence of those metals in the biomass. Soils relate their source to the mine, especially at sampling sites where vegetation grows over the surface of tailings [42]. For the more distant sites, however, this metal enrichment could be related to eolian transportation of dust from the mine during the dry season, when the wind intensity and velocity increase.

4. Conclusions

In the Pan de Azúcar mine, tailings were exposed to weathering for 25 years and developed a 50 cm thick oxidation zone, where jarosite $(Na,K,Pb)Fe_3(SO_4;AsO_4)_2(OH)_6$ is the main secondary Fe^{3+} phase. Jarosite immobilized arsenic and lead inside the tailings. The presence of schwertmannite is also suggested, favoring additionally arsenic immobilization. The primary zone has 9.5 wt % of pyrite-marcasite content and a SNNP = −318.73. The precipitation of anglesite, wupatkite and gypsum retain Pb, Co, and Ca, while Fe^{2+}, Zn, Al, Mg, Cd, As, and other metals migrate downwards, forming a sulfate and metal rich plume. The plume outcrops at the base of DC2, where during the dry season, evaporation mainly favors melanterite ($(Fe^{2+},Zn^{2+})SO_4 \cdot 7H_2O$) and alunogen ($Al_2(SO_4)_3 \cdot 17H_2O$) formation.

Iron is the fourth most abundant metal in the water-soluble phases of the tailings. In the erosion channel of DC2, the formation of sulfate and Fe rich efflorescent salts dominates during the dry season through their exposure to high evaporation. In the oxidation and transition zones, where Fe^{3+} is the dominant species, most of the efflorescent salts are rich in Fe^{3+}, such as rhomboclase ($(H_3O)Fe^{3+}(SO_4)_2 \cdot H_2O$), coquimbite ($Fe^{3+}(SO_4)_3 \cdot 9H_2O$), and copiapite ($Fe^{2+}Fe_4^{3+}(SO_4)_6(OH)_2 \cdot 20H_2O$). In the primary zone, Fe^{2+} precipitates as szomolnokite ($Fe^{2+}SO_4 \cdot H_2O$).

In the acid water that drains from DC1 and DC2, SO_4^{2-}, Fe, Zn, Al, Ca, Mg, Cu, and As are the most abundant compounds. The acid pond shows the highest concentration in those elements at the beginning of wet season, when the soluble salts and jarosite dissolve.

On the surface of the CN tailings impoundment, the formation of efflorescent salt formation results from capillary transport, but in DC1 and DC2, the presence of the coarser alluvial layer that covers the tailings prevents the formation of efflorescent salts on the surface. Nevertheless, the upper layer does not prevent the infiltration of rain water during the wet season, which allows the oxidation of sulfides, and subsequent metal and acidity release, and secondary mineral formation.

Acknowledgments

We acknowledge the support of a PhD fellowship Consejo Nacional de Investigaciones Científicas y Técnicas-Universidad Nacional de Salta (CONICET-UNSa). Consejo de Investigaciones de la Universidad Nacional de Salta (CIUNSA) projects numbered: 1859 and 1674 and Conicet Project: PIP 201101-00189. Province of Jujuy Mining Secretary and local members from the communities of Pan de Azúcar, Ciénego Grande, and the area near the Pan de Azúcar mine. We especially thank Ana Julia Sandobal, Marcos Bernuchi, Cristian Mamani, Gustavo Soria and the Administration from Pozuelos Reserve-APN (Administración de Parques Nacionales), for the support in the field campaigns.

Author Contributions

Jesica Murray, Alicia Kirschbaum and Bernhard Dold sheared the field geological work and the geochemical and mineralogical interpretation of the system. Edi Mendes Guimaraes and Elisa Panunzio Miner were involved in the mineralogical characterization and interpretation in the X-ray diffraction laboratories.

Conflicts of Interest

The authors declare no conflicts of interest.

References

1. Nordstrom, D.K.; Alpers, C.N. Negative pH, efflorescent mineralogy, and consequences for environmental restoration at the Iron Mountain Superfund site, California. *Proc. Natl. Acad. Sci. USA* **1999**, *96*, 3455–3462.
2. Jambor, J.L.; Nordstrom, D.K.; Alpers, C.N. Metalsulphate salts from sulphide mineral oxidation. *Rev. Mineral. Geochem.* **2000**, *40*, 303–350.

3. Bea, S.A.; Ayora, C.; Carrera, J.; Saaltink, M.W.; Dold, B. Geochemical and environmental controls on the genesis of efflorescent salts on coastal mine tailings deposits: A discussion based on reactive transport modeling. *J. Contam. Hydrol.* **2010**, *111*, 65–82.
4. Dold, B. Element flows associated with marine shore mine tailings deposits. *Environ. Sci. Technol.* **2006**, *40*, 752–758.
5. lpers, C.N.; Nordstrom, D.K.; Thompson, M.J. Seasonal variations in Zn/Cu ratios in acid mine water from Iron Mountain, California. In *Environmental Geochemistry of Sulphide Oxidation*; Alpers, C.N., Blowes, D.W., Eds.; ACS Publications: Washington, DC, USA, 1994; Volume 550, pp. 324–344.
6. Hammarstrom, J.M.; Seal, R.R., II; Meier, A.L.; Kornfeld, J.M. Secondary sulphate minerals associated with acid drainage in the eastern US: Recucling of metals and acidity in surficial environments. *Chem. Geol*. **2005**, *215*, 407–431.
7. Nordstrom, D.K.; Alpers, C.N. Geochemistry of acid mine waters. In *The Environmental Geochemistry of Mineral Deposits*; Plumlee, G.S., Logsdon, M.J., Eds.; Society of Economic Geologists: Littleton, CO, USA, 1999; Volume 6A, pp. 133–160.
8. Hudson, E. Sources, mineralogy, chemistry and fate of heavy metal-bearing particles in mining-affected river systems. *Mineral. Mag.* **2003**, *2*, 205–217.
9. Dold, B.; Fontbote, L. Element cycling and secondary mineralogy in porphyry copper tailings as a function of climate, primary mineralogy, and mineral processing. *J. Geochem. Explor*. **2001**, *74*, 3–55.
10. Jamieson, H.E.; Robinson, C.; Alpers, C.N.; McCleskey, R.B.; Nordstrom, D.K.; Peterson, R.C. Major and trace element composition of copiapite-group minerals and coexisting water from the Richmond mine, Iron Mountain, California. *Chem. Geol*. **2005**, *215*, 387–405.
11. Bigham, J.M.; Carlson, L.; Murad, E. Schwertmannite, a new iron oxyhydroxy-sulphate from Pyhäsalmi, Finland, and other localities. *Mineral. Mag*. **1994**, *58*, 641–648.
12. Bigham, J.M.; Nordstrom, D.K. Iron and aluminum hydroxysulphates from acid sulphate water. In *Sulphate Minerals: Crystallography, Geochemistry, and Environmental Significance*; Alpers, C.N., Jambor, J.L., Nordstrom, D.K., Eds.; Reviews in Mineralogy and Geochemistry Volume 40; Mineralogical Society of America: Chantilly, VA, USA, 2000; Volume 40, pp. 351–403.
13. Dutrizac, J.E.; Jambor, J.L. Jarosites and their application in hydrometallurgy. In *Sulphate Minerals: Crystallography, Geochemistry, and Environmental Significance*; Alpers, C.N., Jambor, J.L., Nordstrom, D.K., Eds.; Reviews in Mineralogy and Geochemistry Volume 40; Mineralogical Society of America: Chantilly, VA, USA, 2000; pp. 405–443.
14. Stoffregen, R.E.; Alpers, C.; Jambor, J.L. Alunite-jarosite cristalography, thermodynamics and geochonolology. In *Sulphate Minerals: Crystallography, Geochemistry, and Environmental Significance*; Alpers, C.N., Jambor, J.L., Nordstrom, D.K., Eds.; Reviews in Mineralogy and Geochemistry Volume 40; Mineralogical Society of America: Chantilly, VA, USA, 2000; pp. 454–475.
15. Hudson-Edwards, K.A.; Wright, K. Computer simulations of the interactions of the (0 1 2) and (0 0 1) surfaces of jarosite with Al, Cd, Cu^{2+} and Zn. *Geochim. Cosmochim. Acta* **2011**, *75*, 52–62.

16. Kirschbaum, A.; Murray, J.; Arnosio, M.; Tonda, R.; Cacciabue, L. Pasivos ambientales mineros en el noroeste de Argentina: Aspectos mineralógicos. Geoquímicos y consecuencias ambientales. *Rev. Mex. Cienc. Geol.* **2012**, *29*, 248–264. (In Spanish)
17. McGlue, M.M.; Ellis, G.S.; Cohen, A.S.; Swarzenski, P.W. Palya-lake sedimentation and organic matter accumulation in an Andean piggyback basin: The recent record from the Cuenca de Pozuelos, North-West Argentina. *Sedimentology* **2012**, *59*, 1237–1256.
18. Bianchi, A.R.; Yañez, C.E.; Acuña, L.R. Bases de Datos Mensuales de Precipitaciones del Noroeste Argentino. Available online: http://inta.gob.ar/documentos/las-precipitaciones-del-noroeste-argentino-periodo-1934-1990/ (accessed on 28 May 2014).
19. Legates, D.R.; Willmott, C.J. Mean seasonal and spatial variability in gauge-corrected, global precipitation. *Int. J. Climatol*. **1990**, *10*, 111–127.
20. Legates, D.R.; Willmott, C.J. Mean seasonal and spatial variability in global surface air temperature. *Theor. Appl. Climatol*. **1990**, *41*, 11–21.
21. Segal, S.J. Estudio mineralógico y consideraciones genéticas del distrito minero "Pan de Azúcar", Departamento Rinconada, provincia de Jujuy. *Rev. Asoc. Geol. Argent.* **1980**, *35*, 375–400. (In Spanish)
22. Caffe, P.; Coira, B.L. Complejos de domos volcánicos del mioceno medio de Puna Norte. Un modelo geológico y metalogenético para yacimientos de metales de base ricos en plata (estaño). In *Recursos Minerales de la República Argentina*; Zappettini, E.O., Ed.; Instituto de Geología y Recursos Minerales, Servicio Geológico Minero Argentino: Buenos Aires, Argentina, 1999; Volume 35, pp. 1569–1578. (In Spanish)
23. Segal, S.J.; Caffe, P.J. El grupo minero Pan de Azúcar, Jujuy. In *Recursos Minerales de la República Argentina*; Zappettini, E.O., Ed.; Instituto de Geología y Recursos Minerales, Servicio Geológico Minero Argentino: Buenos Aires, Argentina, 1999; Volume 35, pp. 1579–1592. (In Spanish)
24. Jackson, M.L. *Análisis Químico de Suelos*; Omega: Barcelona, Spain, 1976. (In Spanish)
25. Jambor, J.L. Mineralogy of sulphide-rich tailings and their oxidation products. In *The Environmental Geochemistry of Sulphide Mine-Waste*; Blowes, D.W., Jambor, J.L., Alpers, C.N., Eds.; Mineralogical Association of Canada: Quebec, QC, Canada, 1994; pp. 59–102.
26. Dold, B. Speciation of the most soluble phases in a sequential extraction procedure adapted for geochemical studies of copper sulphide mine waste. *J. Geochem. Explor.* **2003**, *80*, 55–68.
27. Jamieson, H.E.; Robinson, C.; Alpers, C.N.; Nordstrom, D.K.; Poustovetov, A.; Lowers, H.A. The composition of coexisting jarosite-group minerals and water from the richmond mine, iron mountain, California. *Can. Mineral*. **2005**, *43*, 1225–1242.
28. Burton, E.; Bush, R.; Johnston, S.; Watling, K.; Hocking, R.; Sullivan, L.; Parker, G. Sorption of Arsenic(V) and Arsenic(III) to Schwertmannite. *Environ. Sci. Technol.* **2009**, *43*, 9202–9207.
29. Dold, B.; Wade, C.; Fontboté, L. Water management for acid mine drainage control at the polymetallic Zn-Pb-(Ag-Bi-Cu) deposit of Cerro de Pasco, Peru. *J. Geochem. Explor*. **2009**, *100*, 133–141.
30. Moore, D.M.; Reynolds, R.C. *X-ray Difraction and the Identification and Analysis of Clay Minerals*, 2nd ed.; Oxford University Press: Oxford, UK, 1997.

31. Dold, B.; Blowes, D.W.; Dickhout, R.; Spangenberg, J.E.; Pfeifer, H.R. Low molecular weight carboxylic acids in oxidizing sulphide mine tailings. *Environ. Sci. Technol.* **2005**, *39*, 2515–2521.
32. Dold, B.; Gonzalez-Toril, E.; Aguilera, A.; Lopez-Pamo, E.; Cisternas, M.-E.; Amils, R. Acid rock drainage and rock weathering in Antarctica—Important sources for iron cycling in the Southern Ocean. *Environ. Sci. Technol.* **2013**, *47*, 6129–6136.
33. Merwin, H.E.; Posnjak, E. Sulphate incrustations in the Copper Queen Mine, Bisbee, Arizona. *Am. Mineral*. **1937**, *22*, 567–571.
34. Smuda, J.; Dold, B.; Spangenberg, J.E.; Bustos, C.; Kobek, M.; Pfeifer, H.-R. Element cycling during the transition from alkaline to acidic environment in an active porphyry copper tailings impoundment, Chuquicamata, Chile. *J. Geochem. Explor.* **2014**, *140*, 23–40.
35. Smith, A.M.; Dubbin, W.E.; Wright, K.; Hudson-Edwards, K.A. Dissolution of lead- and lead-arsenic-jarosites at pH 2 and 8 and 20 °C: Insights from batch experiments. *Chem. Geol.* **2006**, *229*, 344–361.
36. Kendall, M.; Madden, A.S.; Elwood Madden, E.M.; Hu, Q. Effects of arsenic incorporation on jarosite dissolution rates and reaction products. *Geochim. Cosmochim. Acta* **2013**, *112*, 192–207.
37. Hudson-Edwards, K.A.; Schell, C.; Macklin, M.G. Mineralogy and geochemistry of alluvium contaminated by metal mining in the Rio Tinto area, southwest Spain. *Appl. Geochem*. **1999**, *14*, 55–70.
38. Taylor, M.P.; Hudson-Edwards, K.A. The dispersal and storage of sediment-associated metals in an arid river system: The Leichhardt River, Mount Isa, Queensland, Australia. *Environ. Pollut.* **2008**, *152*, 193–204.
39. Kirschbaum, A.; Murray, J.; López, E.; Equiza, A.; Arnosio, M.; Boaventura, G. The environmental impact of Aguilar mine on the heavy metalconcentrations of the Yacoraite River, Jujuy Province, NW Argentina. *Environ. Earth Sci.* **2012**, *65*, 493–504.
40. Murray, J.; Kirschbaum, A.; Dold, B. Acid mine drainage from Pan de Azúcar Mine (Zn-Pb-Ag) and possible Arsenic input on the water quality of Pozuelos Lagoon Basin, Northwest Argentina. In Proceedings of 1st International Conference on Mine Water Solution in Extreme Environments, Lima, Peru, 15–17 April 2013; pp. 342–350.
41. Hudson-Edwards, K.A.; Archer, J. Geochemistry of arsenic (As) in spring and stream waters from San Antonio de los Cobres, NW Argentina. *Mineral. Mag.* **2008**, *72*, 425–427.
42. Plaza Cazón, J.; Benítez, L.; Murray, J.; Kirschbaum, A.; Kirschbaum, P.; Donati, E. Environmental impact on soil, water and plants from the abandoned Pan de Azúcar Mine. *Adv. Mater. Res*. **2013**, *825*, 88–91.